Metabolism is a major driver of hydrogen isotope fractionation recorded in tree-ring glucose of *Pinus nigra*

Thomas Wieloch[1] (iD)**, Michael Grabner**[2] (iD)**, Angela Augusti**[3] (iD)**, Henrik Serk**[1] (iD)**, Ina Ehlers**[1]**, Jun Yu**[4] (iD) **and Jürgen Schleucher**[1] (iD)

[1]Department of Medical Biochemistry and Biophysics, Umeå University, 901 87 Umeå, Sweden; [2]Institute of Wood Technology and Renewable Materials, University of Natural Resources and Life Sciences Vienna, 3430 Tulln an der Donau, Austria; [3]Research Institute on Terrestrial Ecosystems, National Research Council, Porano (TR) 05010, Italy; [4]Department of Mathematics and Mathematical Statistics, Umeå University, 901 87 Umeå, Sweden

Summary

- Stable isotope abundances convey valuable information about plant physiological processes and underlying environmental controls. Central gaps in our mechanistic understanding of hydrogen isotope abundances impede their widespread application within the plant and bio-geosciences.
- To address these gaps, we analysed intramolecular deuterium abundances in glucose of *Pinus nigra* extracted from an annually resolved tree-ring series (1961–1995).
- We found fractionation signals (i.e. temporal variability in deuterium abundance) at glucose H^1 and H^2 introduced by closely related metabolic processes. Regression analysis indicates that these signals (and thus metabolism) respond to drought and atmospheric CO_2 concentration beyond a response change point. They explain $\approx 60\%$ of the whole-molecule deuterium variability. Altered metabolism is associated with below-average yet not exceptionally low growth.
- We propose the signals are introduced at the leaf level by changes in sucrose-to-starch carbon partitioning and anaplerotic carbon flux into the Calvin–Benson cycle. In conclusion, metabolism can be the main driver of hydrogen isotope variation in plant glucose.

Introduction

Stable isotope measurements of the most abundant chemical elements in plants (H and C) convey valuable information about plant physiological and environmental processes. Plant archives, such as tree rings, preserve this information over millennia enabling elucidation of physiological and environmental dynamics that occur beyond the short time frames covered by manipulation or monitoring experiments (Loader *et al.*, 2011; Peñuelas *et al.*, 2011; Saurer *et al.*, 2014; Frank *et al.*, 2015; Köhler *et al.*, 2016).

Among all stable isotopes, the hydrogen isotopes protium (^{1}H) and deuterium (^{2}H or D) exhibit the largest relative mass difference. As a result, hydrogen isotope effects are normally considerably larger than isotope effects of other elements (Melander & Saunders, 1980). Thus, from the physics point of view, hydrogen isotope compositions of plant compounds (commonly expressed in terms of δD) have a remarkable potential to further our knowledge about plant physiological and environmental processes. However, current plant δD models fail to predict the entire body of available empirical data (see later). Therefore, hydrogen isotopes, in contrast to carbon isotopes, have not yet evolved into standard tools within the plant and biogeosciences.

Current δD models of plant organic matter exhibit three main components: (1) the δD composition of plant water sources; (2) leaf water D enrichment; and (3) metabolic fractionations. (1) Plants take up soil water through roots. In most plants, this uptake and water transport through the xylem into leaves occur without detectable δD shifts (Cernusak *et al.*, 2016; Chen *et al.*, 2020). Additionally, leaf water exchanges with atmospheric water vapour through stomata. Thus, leaf water inherits the δD compositions of both soil water and atmospheric water vapour (Cernusak *et al.*, 2016). (2) Stomatal evaporation causes D enrichment in leaf water. Adaptations of the Craig–Gordon model describe this process at the site of evaporation (Craig & Gordon, 1965; Flanagan *et al.*, 1991; Farquhar *et al.*, 2007). In a comprehensive series of gas exchange experiments over a range of isotopic and humidity conditions far exceeding natural conditions, Roden & Ehleringer (1999a) confirmed the robustness of a model that approximates leaf water D enrichment (Flanagan *et al.*, 1991). Similarly, on an extensive δD data set of leaf waters from very dry to very wet field sites, Kahmen *et al.* (2013) confirmed the robustness of the precise δD enrichment model (Farquhar *et al.*, 2007). Reanalysing this latter data set, Cernusak *et al.* (2016) reported a goodness of fit of $R^2 = 0.92$ ($n = 332$) between modelled and measured δD data. These successful tests

for robustness of leaf water δD models strongly suggest that inconsistencies between modelled and measured δD values of plant organic matter as reported by Waterhouse *et al.* (2002) derive from processes that occur downstream of leaf water D enrichment, that is from fractionating metabolic processes. (3) Yakir & DeNiro (1990) developed a δD model describing fractionation in cellulose of aquatic plants and estimated metabolic fractionation factors of autotrophic and heterotrophic growth. To predict δD values of tree-ring cellulose, Roden *et al.* (2000) combined this model with a leaf water δD model (Flanagan *et al.*, 1991) and added a term accounting for δD changes by partial reincorporation of hydrogen from xylem water during cellulose biosynthesis (=heterotrophic hydrogen exchange). Roden & Ehleringer (1999b, 2000) confirmed the robustness of their model for glasshouse- and field-grown riparian trees with good access to water. A robustness test by Waterhouse *et al.* (2002) on tree rings of *Quercus robur* from a dry site failed. These latter authors suggested modelling metabolic fractionations as constants may be inadequate.

All hydrogen positions of leaf-level metabolites inherit D fractionations present in leaf water, the hydrogen source of metabolism. By contrast, metabolic reactions cause D fractionations at specific intramolecular hydrogen positions that are directly or indirectly involved in the reaction mechanism (Schmidt *et al.*, 2015). Such fractionations are known to result in pronounced δD differences among hydrogen positions within a metabolite (Martin *et al.*, 1986; Schleucher, 1998; Schmidt *et al.*, 2003). Furthermore, it is now known that metabolic δD variability can occur at a given intramolecular hydrogen position (Schleucher, 1998). Specifically, δD variability at H^6 of plant leaf glucose was explained by changes in the photorespiration-to-photosynthesis ratio (Schleucher, 1998; Ehlers *et al.*, 2015). Moreover, growing six C_3 species at ambient CO_2 concentrations of 280 and 150 ppm, Cormier *et al.* (2018) reported whole-molecule δD differences of $\approx 20‰$ (on average) in leaf α-cellulose due to unknown fractionating metabolic processes. This shows the predictive abilities of plant δD models will improve by accounting for variability in metabolic fractionations. To this end, however, underlying mechanisms need to be elucidated.

Based on findings by Waterhouse *et al.* (2002), we hypothesise metabolic processes manifest significant fractionation signals (throughout the paper, the term 'signal' denotes temporal variability in deuterium abundance) at carbon-bound hydrogens in tree-ring glucose under dry conditions. Since metabolic fractionations occur at specific hydrogen positions within molecules, the interpretability of conventional whole-molecule data is fundamentally limited. For instance, not knowing the intramolecular location of metabolic fractionation impedes attempts to elucidate its enzymatic origin. Additionally, if located at a single hydrogen position, a *c.* 20‰ whole-molecule effect scales up to *c.* 140‰ because glucose has seven H-C positions. Therefore, to test our hypothesis, we measured intramolecular D abundance in tree-ring glucose of *Pinus nigra* from a dry site in the Vienna region. This region was chosen for its comprehensive environmental monitoring. We first screen for metabolic fractionation signals. Then, we analyse signal–environment and signal–growth

relationships and estimate the contribution of metabolic to whole-molecule fractionation. Lastly, we discuss mechanisms of signal introduction and implications of our findings for isotope studies in the plant and biogeosciences.

Materials and Methods

Site and samples

Pinus nigra Arnold was sampled at Bierhäuselberg, Vienna region, Austria (48.13°N, 16.23°E, 350 m amsl). The site exhibits shallow, very dry soil and an open canopy with apparently low competition among trees (Leal *et al.*, 2008). Sampling targeted dominant trees with umbrella-shaped crowns indicating regular water shortage. From each of 19 specimens (age range: *c.* 92–156 yr), two 5-mm stem cores were taken at breast height. Individual tree rings were dated by standard dendrochronological methods (Speer, 2010) and separated using a binocular microscope and a scalpel. To preclude growth-related isotope signals, we analysed tree rings formed from 1961 to 1995 when all trees had reached a comparably stable canopy position. Across trees, all tree-ring material of a given year was combined into annual pools yielding one sample per year. Thus, analytical results represent properties of the tree species at the site rather than individual trees.

### Intramolecular deuterium measurements

After sample randomisation, intramolecular D abundances of glucose were measured following a published protocol (Betson *et al.*, 2006). Samples < 20 mg were excluded from analysis (1977, 1978, 1981 and 1982), because too much measurement time would have been required for sufficient precision. Quantitative D NMR spectra ($n \geq 3$) were recorded using an AVANCE III 850 with a cryogenic probe optimised for D detection and ^{19}F lock (Bruker BioSpin GmbH, Rheinstetten, Germany). Relative intramolecular D abundances were determined by signal deconvolution using Lorentzian line shape fits in TopSpin 4 (Bruker BioSpin GmbH, Rheinstetten, Germany). 3,6-Anhydro-1,2-*O*-isopropylidene-α-D-glucofuranose has six methyl group hydrogens, which were introduced during derivatisation and were derived from a common batch of acetone. Their D abundance (arithmetic mean) was used as reference to compare glucose D abundances of tree-ring samples from different years as follows:

$$\delta D_i = \frac{D_i}{\Sigma D_{ME}/6} - 1 \qquad \text{Eqn 1}$$

with D_i and D_{ME} denoting relative D abundance at glucose H-C positions (Fig. 1) and the methyl group hydrogens, respectively.

Environmental data

Monthly resolved data of precipitation, *PRE*, air temperature, *TMP*, sunshine duration, *SD*, global radiation, *RAD* and relative humidity were measured at the climate station Hohe Warte (WMO ID: 1103500). Air vapour pressure deficits, *VPD*, were
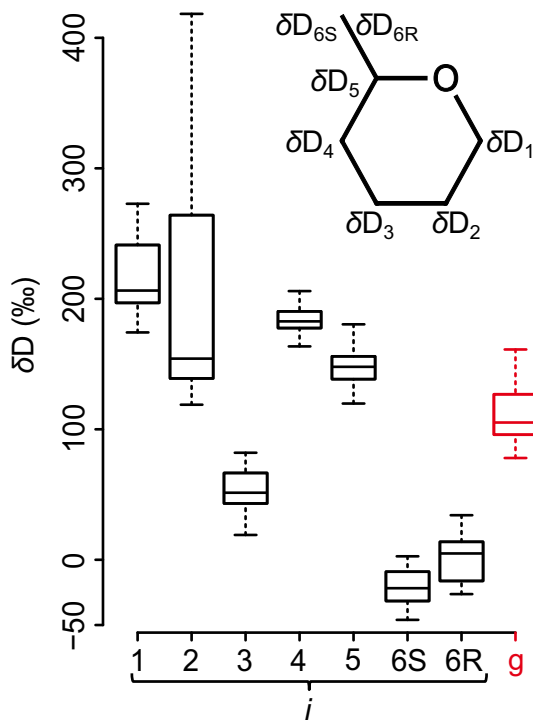
Fig. 1 Variability in δD time series shown by boxplots. δD_i and δD_g denote time series of D abundance at intramolecular H-C positions in tree-ring glucose (black) and of the whole molecule (red), respectively. Data were acquired for tree-ring glucose of *Pinus nigra* laid down from 1961 to 1995 at a site in the Vienna Basin (δD_i: $\pm SE = 5.4‰$, $n \geq 3$; δD_g: $\pm SE = 3.4‰$, $n \geq 3$). Outliers were removed before analysis (δD_1 to δD_3: $n = 31$; δD_4 and δD_5: $n = 30$; δD_{6S}: $n = 26$; δD_{6R}: $n = 28$; and δD_g: $n = 25$). Data reference: Average D abundance of the methyl group hydrogens of the glucose derivative used for NMR measurements. Insert: glucose carbon skeleton showing intramolecular locations of δD_i time series.

calculated according to published procedures (Abtew & Melesse, 2013). We used monthly resolved data sets of the self-calibrating Palmer drought severity index, *PDSI*, and the standardised precipitation–evapotranspiration index, *SPEI*, for 48.25N, 16.25E (Wells *et al.*, 2004; Vicente-Serrano *et al.*, 2010). Annual atmospheric CO_2 concentrations, C_a, were measured at the Mauna Loa Observatory, Hawaii, by Pieter Tans (NOAA/ESRL, Boulder, CO, USA) and Ralph Keeling (Scripps Institution of Oceanography, La Jolla, CA, USA). Both the selected grid point and climate station are no more than a horizontal distance of 15 km from the sampling site with a negligible vertical offset. CO_2 is well mixed in the atmosphere. Thus, all data should represent the site conditions well.

Statistical analyses

We calculated the variance contribution of each intramolecular D time series, δD_i, to the whole-molecule D time series, δD_g, as follows:

$$\delta D_g = \frac{\Sigma \delta D_i}{7} \qquad \text{Eqn 2}$$

with the variance of δD_g equal to the covariance average between δD_i and δD_g as

$$\text{Var}(\delta D_g) = \frac{\Sigma \text{Cov}(\delta D_i, \delta D_g)}{7} \qquad \text{Eqn 3}$$

Thus, variance contributions of δD_i to δD_g are given as

$$\text{VC}_i = \frac{\text{Cov}(\delta D_i, \delta D_g)}{7 \times \text{Var}(\delta D_g)} \qquad \text{Eqn 4}$$

See Supporting Information Notes S1 for information on other statistical analyses.

Results

To better understand metabolic fractionations, we measured intramolecular D abundances at all seven H-C positions of glucose extracted across an annually resolved *Pinus nigra* tree-ring series (Fig. 1). Our time series cover the period from 1961 to 1995 but lack data for 1977, 1978, 1981 and 1982. Hence, the data set consists of seven intramolecular δD_i time series each comprising 31 observations ($n = 7 \times 31 = 217$). Additionally, we derived the molecular average time series, δD_g ($n = 31$).
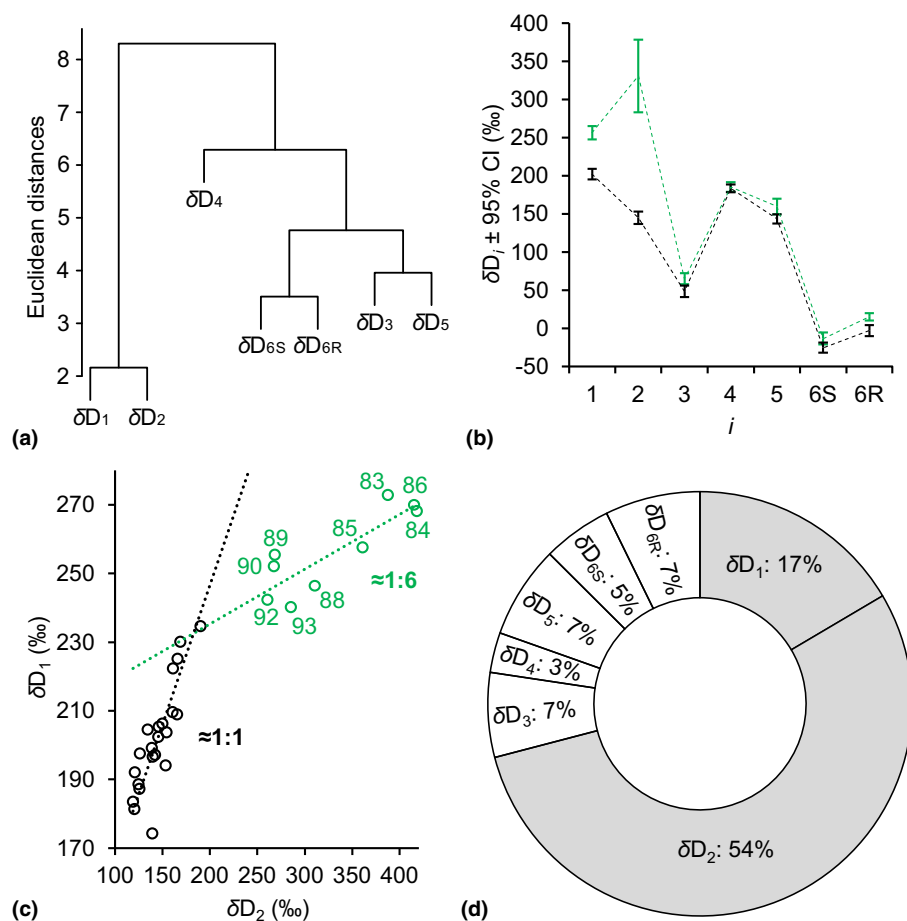
Outlier analysis

Outliers can potentially impair statistical analyses because they may reflect either experimental errors or extreme states of the system. Since we were interested in the normal functioning of plant metabolism and metabolic fractionation, we removed outliers to ensure robust statistical results. We identified outliers in δD_i time series ($n = 31$) as values that were 1.5 times the interquartile range below the first or above the third quartile. We removed one data point each from δD_4 and δD_5 ($n = 30$), three data points from δD_{6R} ($n = 28$) and five data points from δD_{6S} ($n = 26$) resulting in six missing data points in δD_g ($n = 25$). The average standard errors of δD_i and δD_g measurements are 5.4‰ and 3.4‰, respectively.

δD_1 and δD_2 reflect highly variable and closely related metabolic processes

Intramolecular D abundances of *Pinus nigra* tree-ring glucose differ among H-C positions (Figs 1, 2b; Notes S2). Medial intramolecular differences exceed 225‰ (δD_1 vs δD_{6S}). This shows that metabolic fractionations, being position-specific, have strong effects. Interestingly, in some years, intramolecular δD differences approach 450‰ (Notes S2). Thus, metabolic fractionations are highly variable on the interannual scale.

Hierarchical cluster analysis (HCA) groups time series according to covariability. Time series carrying common signals, that is information about a common process or strongly related processes, form clusters. Performing HCA on our δD_i data set, we found a strong separation between a cluster comprising δD_1 and

Fig. 2 (a) Common variability in δD_i time series detected by hierarchical cluster analysis (HCA). (b) Intramolecular δD_i patterns of the low- and high-value groups (black and green, respectively). (c) Relationship between δD_1 and δD_2 (overall $R^2 = 0.93$, $P < 10^{-15}$, $n = 31$). Dotted lines: linear major axis regression models showing that δD_1 and δD_2 increase at a 1 : 1 ratio at low values (black) and at a 1 : 6 ratio at high values (green). (d) Per cent contributions of δD_i to the variance in δD_g. δD_i and δD_g denote time series of D abundance at intramolecular H-C positions in tree-ring glucose and of the whole molecule, respectively. Data were acquired for tree-ring glucose of *Pinus nigra* laid down from 1961 to 1995 at a site in the Vienna Basin (δD_i: $\pm SE = 5.4$‰, $n \geq 3$; δD_g: $\pm SE = 3.4$‰, $n \geq 3$). Outliers were removed before analysis (δD_1 to δD_3: $n = 31$; δD_4 and δD_5: $n = 30$; δD_{6S}: $n = 26$; δD_{6R}: $n = 28$; and δD_g: $n = 25$). Low- and high-value groups were identified by HCA (Supporting Information Notes S2). Fig. 2(b) shows discrete data. Dashed lines were added to guide the eye. The variance partitioning analysis (2d) is based on years without missing data after removing outliers ($n = 8 \times 25$). Data reference: Average D abundance of the methyl group hydrogens of the glucose derivative used for NMR measurements.

δD_2 and a cluster comprising δD_3 to δD_{6R} (Fig. 2a). Additionally, we found separations within the δD_3 to δD_{6R} cluster, with δD_4 showing the highest degree of independency. Thus, δD_i time series carry information about several fractionation processes.

While δD_3 to δD_{6R} exhibit similar degrees of variability (Fig. 1; SD = ±10.5‰ to ±16.8‰, range = 42‰ to 63‰, $n = 26$–31), δD_2 varies considerably (SD = ±91.8‰, range = 300‰, $n = 31$) and δD_1 is also relatively variable (SD = ±28.4‰, range = 99‰, $n = 31$). Increased D variability at two out of seven H-C positions indicates highly variable metabolic fractionations at these positions, H^1 and H^2.

To further investigate this, we performed HCA on annual δD_i patterns and found two groups (Notes S2). Fig. 2(b) shows the arithmetic average patterns of both groups. While δD_3 to δD_{6R} values remain comparably constant under all conditions experienced by the trees, δD_1 and δD_2 separate annual δD_i patterns into a low-value group (black, $n = 22$) and a high-value group (green, $n = 9$). Average and median increases in δD_1 and δD_2 are statistically significant (one-tailed Student's t-tests: δD_1, $P < 10^{-9}$; δD_2, $p < 10^{-4}$; one-tailed Mood's median tests: δD_1 and δD_2, $P < 0.001$). Since differences in δD_i patterns reflect differences in metabolism, this finding confirms that glucose H^1 and H^2 carry exceptionally variable metabolic fractionation signals. Underlying metabolic processes are closely related (Fig. 2a).

Nonmetabolic fractionation processes (e.g. leaf water D enrichment) have equal effects on all δD_i. In regression analysis

investigating relationships among different δD_i, these processes can be expected to yield slopes = 1. By contrast, metabolic fractionation processes affect subsets of δD_i and may thus cause deviations from slope = 1. To investigate which kind of fractionation shapes the variation in the low- and high-value groups, we performed major axis regression analysis on low and high δD_1 and δD_2 values (Fig. 2c, black and green circles, respectively). Compared with ordinary least squares regression analysis, major axis regression analysis yields truer parameter estimates when x-variable data contain significant relative errors as is the case here for low-value data. For low values, we found a slope of c. 0.81 with a 95% confidence interval of c. 0.60 to c. 1.07 ($n = 22$); that is, δD_1 and δD_2 increase at a c. 1 : 1 ratio. For high values, we found a slope of c. 0.16 with a 95% confidence interval of c. 0.07 to c. 0.25 ($n = 9$); that is, δD_1 and δD_2 increase at a c. 1 : 6 ratio. Thus, while δD_1 and δD_2 variability in the low-value group is consistent with expectations related to non-metabolic fractionation processes, high δD_1 and δD_2 values reflect additional effects by metabolic fractionation processes.

Metabolism changes in response to dry conditions after a change point is crossed

To investigate the controls of the metabolic fractionation processes, we estimated metabolic fractionation at glucose H^1 and H^2 as

$$\varepsilon_{met} = \frac{1/2\Sigma(D_1, D_2)}{1/5\Sigma(D_3, D_4, D_5, D_{6S}, D_{6R})} - 1 \qquad \text{Eqn 5}$$

where D_i denotes relative D abundance at glucose H-C positions (Fig. 1). This procedure maximises metabolic fractionation signals located at H^1 and H^2, removes fractionation signals equally present at all H-C positions (leaf water D enrichment) and minimises signals of processes affecting all H-C positions similarly (heterotrophic hydrogen exchange). Weaker metabolic fractionation signals present at glucose H^3 to H^6 (Figs 1, 2a) will be further explored in future analyses of the data set.

In general, the fractionating metabolic processes may be under developmental control (Gray & Song, 1984). However, the formation of tree rings analysed here occurred when the trees had reached a stable canopy position. On average, tree-ring width measurements of the samples reach back to 1865 (range: 1840–1918) and δD_i time series start at 1961. Thus, the fractionating metabolic processes can be expected to be controlled by environmental parameters. In the following, these are elucidated in six steps, which motivate two integrated isotope–environment models presented subsequently.

Step 1 Increases in ε_{met} are temporally confined to the second part of the study period (Fig. 2c, 1983–1993). This may indicate the presence of a response change point. To test this, we performed a batch change point analysis based on the nonparametric Mann–Whitney–Wilcoxon test (Ross, 2015). We found a change point at 1980 ($P < 0.001$, $n = 31$), showing that the observed frequency distribution of ε_{met} (Notes S3) does not align with the properties of a single theoretical probability distribution. That is, ε_{met} data of 1961–1980 and 1983 to 1995 follow different probability distributions (1981 and 1982 are missing). Thus, the ε_{met} time series exhibits a change point beyond which the fractionating metabolic processes are activated or upregulated.

Step 2 Upregulation of the fractionating metabolic processes occurs beyond a change point. Before the change point, environmental variability exerts no significant control (Fig. 2c, 1 : 1 ratio). To investigate when the change point is crossed, we

correlated ε_{met} with different climate parameters. Since ε_{met} does not follow a normal distribution (Notes S3), we calculated Spearman's rank correlation coefficient, ρ. Our analysis included four time periods: January to December, year; March to May, spring; March to November, growing season (Wieloch et al., 2018); and June to July, summer. For most periods, we found significant positive correlations of ε_{met} with VPD and significant negative correlations with PDSI and SPEI (Table 1). High VPD, low PDSI and low SPEI correspond to dry conditions. Thus, the results indicate that upregulation of the fractionating metabolic processes (high ε_{met}) occurs in response to dry conditions.

Step 3 SPEI can be calculated for different timescales indicating different types of hydrological drought (Vicente-Serrano et al., 2010). While short timescales indicate variability in soil moisture, long timescales indicate variability in groundwater storage (Vicente-Serrano et al., 2010). To investigate the effects of different drought types on the fractionating metabolic processes, we correlated ε_{met} with SPEI calculated for timescales of 1, 3, 4, 6, 8, 12, 16, 24, 36 and 48 months. We found increasing correlation coefficients from short to long timescales (Table 1), indicating that long-term drought promoted upregulations of the fractionating metabolic processes (possibly by groundwater depletion). Long-term drought events have a low temporal frequency (Vicente-Serrano et al., 2010). This may explain why upregulations of the fractionating metabolic processes occur not scattered over the entire study period but over consecutive years during the second half of the study period (Fig. 2c).

Step 4 In addition to correlations indicative of drought control, we found a significant positive correlation between ε_{met} and C_a (Table 1), which may constitute a pseudocorrelation resulting from intercorrelation between C_a and long-term drought (Pearson's correlation between C_a and the growing-season 48-month SPEI: $r = -0.83$, $P < 10^{-7}$, $n = 31$). For the year and spring, we found significant positive correlations between ε_{met} and TMP (Table 1). Thus, air temperature may contribute to upregulations of the fractionating metabolic processes. Alternatively, the TMP

Table 1 Spearman's rank correlation coefficients and significance levels for relationships between ε_{met} and climate parameters within the period from 1961 to 1995 ($n = 31$).

	VPD	PRE	PDSI	TMP	SD	RAD	C_a	SPEI 1	3	4	6	8	12	16	24	36	48
Year	0.40	0.01	−0.51	0.45	0.12	0.28	0.58	−0.21	−0.25	−0.27	−0.30	−0.37	−0.46	−0.47	−0.58	−0.60	−0.57
Spring	0.54	−0.13	−0.55	0.55	0.09	0.18	–	−0.24	−0.19	−0.15	−0.16	−0.29	−0.34	−0.43	−0.58	−0.54	−0.55
Growing season	0.39	−0.04	−0.50	0.33	0.01	0.24	–	−0.26	−0.21	−0.20	−0.29	−0.31	−0.43	−0.47	−0.59	−0.61	−0.56
Summer	0.28	−0.04	−0.49	0.02	−0.17	0.10	–	−0.09	−0.20	−0.21	−0.25	−0.31	−0.43	−0.41	−0.56	−0.65	−0.55

ε_{met} denotes the average deuterium fractionation by metabolic processes at glucose H^1 and H^2 ($\pm SE = 3.5$‰, $n \geq 3$). Data for the calculation of ε_{met} were acquired for tree-ring glucose of *Pinus nigra* laid down from 1961 to 1995 at a site in the Vienna Basin. Climate parameters: VPD, air vapour pressure deficit; PRE, precipitation; PDSI, the self-calibrating Palmer drought severity index (Wells et al., 2004); TMP, air temperature; SD, sunshine duration; RAD, global radiation; C_a, atmospheric CO_2 concentrations; SPEI, the standardised precipitation–evapotranspiration index calculated for different timescales (1–48 months) (Vicente-Serrano et al., 2010). Integration periods for the calculation of climate parameters: January to December, year; March to May, spring; March to November, growing season (Wieloch et al., 2018); and June to July, summer. Significance levels: < 0.05, light blue/light pink; < 0.01, blue/pink; and < 0.001, dark blue/dark pink.

correlation may be explained by intercorrelation with drought parameters. Overall, long-term drought shows the highest correlation coefficients (Table 1), indicating that it is the most important environmental control. Furthermore, we considered pathogens as a cause for upregulations of the fractionating metabolic processes. The Research Centre for Forests (Vienna, Austria) closely monitors and reports on pathogen status. To our knowledge, there are no reports of major damage by pathogens for the studied *Pinus nigra* stand during the 1980s and the early 1990s. Thus, significant effects of pathogens on upregulations of the fractionating metabolic processes are unlikely. Similarly, effects by forest management interventions are unlikely since the stand is not used economically (Leal *et al.*, 2008). Effects by air pollutants could not be assessed due to limited data availability.

Step 5 To assess the magnitude of the drought shift indicated by correlation, we plotted the growing-season 48-month *SPEI* as function of time (Fig. 3a). Trendline analysis shows a significant increase in drought severity with a long-term shift from 'nondrought' from 1961 to 1978, to 'mild drought' from 1979 to 1988, to 'moderate drought' from 1989 to 1995 according to the classification of drought severity ($R^2 = 0.69$, $P < 10^{-9}$, $n = 35$) (McKee *et al.*, 1993; Vicente-Serrano *et al.*, 2010). Thus, upregulations of the fractionating metabolic processes in between 1983 and 1993 occurred when the study region experienced mild-to-moderate drought. Note that actual conditions at the site may have deviated from regional conditions plotted in Fig. 3(a).
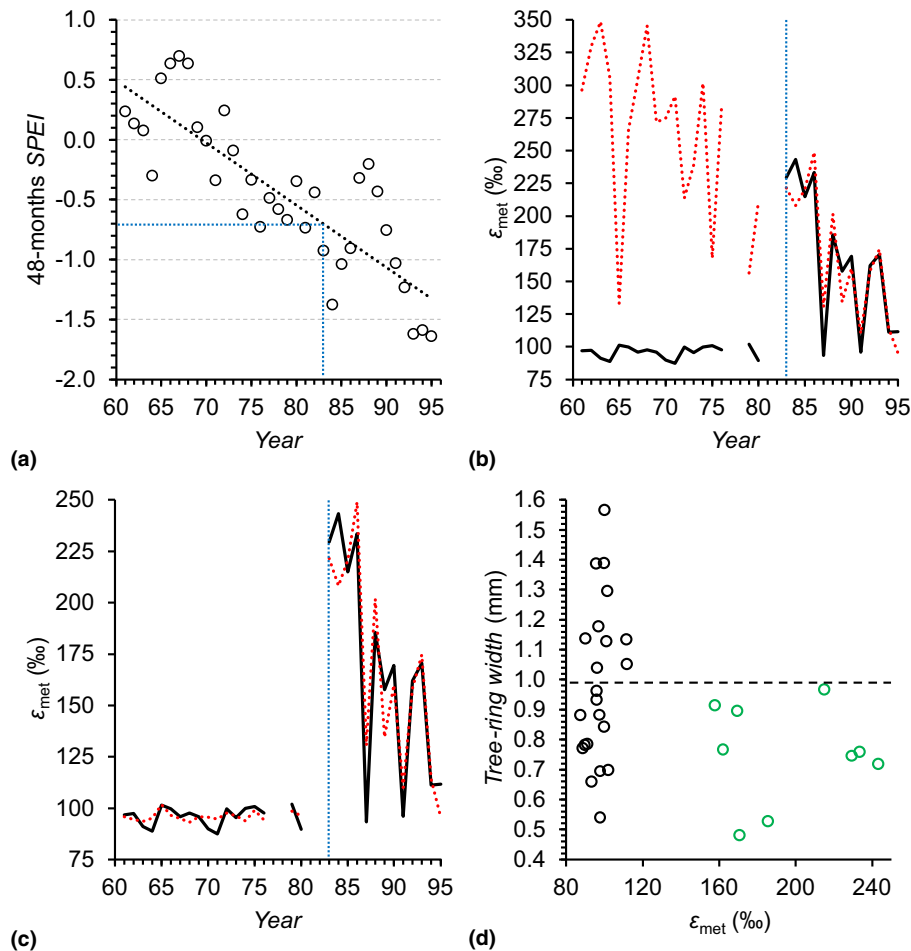
Fig. 3 (a) Long-term development of growing-season drought in the study region. Trendline analysis shows a significant increase in drought severity with shifts from 'nondrought' from 1961 to 1978, to 'mild drought' from 1979 to 1988, to 'moderate drought' from 1989 to 1995 (dotted black line, $R^2 = 0.69$, $P < 10^{-9}$, $n = 35$). *SPEI* denotes the standardised precipitation–evapotranspiration index (Vicente-Serrano *et al.*, 2010). Here, it was calculated for the growing season (March to November (Wieloch *et al.*, 2018)) at 48.25°N, 16.25°E on a 48-month timescale indicative of long-term drought variability (black circles). Expressions of SPEI values indicate the drought severity as ≥−0.49, nondrought; −0.5 to −0.99, mild drought; −1 to −1.49, moderate drought; −1.5 to −1.99, severe drought; and <−2, extreme drought (McKee *et al.*, 1993; Vicente-Serrano *et al.*, 2010). (b, c) Comparison of measured (solid black line) and modelled (dotted red line) metabolic fractionation at glucose H[1] and H[2], ε_{met} ($n = 31$). In (b) and (c), data were modelled by a multivariate linear model (Eqn 6) and a multivariate change point model (Eqn 7; Table 3) (Fong *et al.*, 2017), respectively. Dotted blue line: response change point as determined by the change point model. (d) Relationship between ε_{met} and tree-ring width. Green and black circles: years in which the fractionating metabolic processes were upregulated and downregulated, respectively (Fig. 2). Dashed line: average tree-ring width of years in which the fractionating metabolic processes were downregulated (black circles, 0.99 mm). Tree-ring widths were measured for previous dendro-ecological studies (Leal *et al.*, 2008). Data for the calculation of ε_{met} were acquired for tree-ring glucose of *Pinus nigra* laid down from 1961 to 1995 at a site in the Vienna Basin (±SE = 3.5‰, $n \geq 3$).

Step 6 In 1994 and 1995, long-term drought was exceptionally strong (Fig. 3a). However, this did not result in significant upregulations of the fractionating metabolic processes (Fig. 2c). Therefore, we hypothesise long-term drought beyond a critical level is merely setting the stage for upregulation and secondary climate factors exert control on shorter timescales. To investigate this, we repeated the ε_{met}–climate correlation analysis with data of the second half of the study period, 1983 to 1995. We justify this data selection as follows. In 1983, the upregulation of the fractionating metabolic processes occurred for the first time (Fig. 2c). From 1983 to 1995, long-term drought became more severe (Fig. 3a, dotted black line). Thus, the site conditions during this period may have been generally favourable for upregulation. Before 1983, long-term drought was less severe and may have rendered upregulations impossible (Fig. 3a). In this scenario, control by secondary climate factors would have been impossible and considering their variability would impair correlation results. Since the selected subset of ε_{met} (1983–1995) follows a normal distribution (Notes S3), we calculated Pearson's correlation coefficients, r. We found significant negative correlations between ε_{met} and PRE (Table 2). Under generally dry conditions, low precipitation may result in low soil moisture. Thus, the results indicate that upregulations of the fractionating metabolic processes (high ε_{met}) occurred in response to short-term depletions in soil moisture when long-term drought was beyond the critical level. In this respect, it is noteworthy that *Pinus nigra* reportedly has a well-developed lateral root system in upper soil layers to access soil water but can additionally tap into deep water sources if available (Stokes *et al.*, 2002; Peñuelas & Filella, 2003). Furthermore, we found a significant negative correlation between ε_{met} and annual C_a (Table 2). This correlation is not explained by intercorrelation between C_a and long-term drought (Pearson's correlation between C_a and the growing-season 48-month SPEI: $r = -0.39$, $P > 0.1$, $n = 13$). Thus, the result indicates that high atmospheric CO_2 concentrations counteracted upregulations of the fractionating metabolic processes (high ε_{met}) when long-term drought was beyond the critical level.

Model 1 To further corroborate the existence of a response change point (Step 1), and the requirement of long-term drought (Steps 2 and 3) for the manifestation of effects by secondary climate factors (Step 6), we modelled two ε_{met} groups as functions of PRE and C_a as follows:

$$\varepsilon_{met} = \alpha_1 + \alpha_2 PRE + \alpha_3 C_a \qquad \text{Eqn 6}$$

While the first group includes data from 1961 to 1982 corresponding to less severe long-term drought, the second group includes data from 1983 to 1995 corresponding to more severe long-term drought (Fig. 3a). For the latter group, we found adequate linear models including, as explanatory variables, spring PRE and annual C_a ($R^2 = 0.74$, $P < 0.01$, $n = 13$), and summer PRE and annual C_a ($R^2 = 0.78$, $P < 0.001$, $n = 13$). The most adequate model we found includes summed spring and summer PRE and annual C_a ($R^2 = 0.87$, $P < 10^{-4}$, $n = 13$, $\alpha_1 = 1801.97$, $\alpha_2 = -0.566$, $\alpha_3 = 4.1851$; see Notes S4 for bivariate relationships of ε_{met} with PRE and C_a, respectively). Both PRE and C_a contributed significantly to all models ($P < 0.05$). For ε_{met} data of the first group, 1961 to 1982, the most adequate model has no explanatory power ($P > 0.1$, $n = 18$). Modelling ε_{met} by the most adequate model works well for the second group, 1983–1995, yet produces large offsets between all measured and modelled values of the first group (Fig. 3b). This corroborates that (1) a response change point exists and (2) the manifestation of effects by secondary climate factors requires long-term drought. Furthermore, it should be noted that the most adequate model accounts well for low ε_{met} values in 1994 and 1995 (Fig. 3b). During these years, long-term drought was exceptionally severe, yet PRE and C_a were high (Fig. 3a; Notes S4). Thus, long-term drought alone may not necessarily lead to upregulation of the fractionating metabolic processes. High precipitation during spring and summer, as well as high atmospheric CO_2 concentrations, may exert counteracting effects.

Model 2 Above, we found indications for several properties of ε_{met} of *Pinus nigra* tree-ring glucose. To test these properties in an integrated way and to estimate the change point value, we fitted a change point model to the entire dataset (Fong *et al.*, 2017). It takes the form

Table 2 Pearson's correlation coefficients and significance levels for relationships between ε_{met} and climate parameters within the period from 1983 to 1995 ($n = 13$).

	VPD	PRE	PDSI	TMP	SD	RAD	C_a	SPEI 1	3	4	6	8	12	16	24	36	48
Year	0.26	−0.69	−0.51	−0.17	−0.12	−0.34	−0.73	−0.18	−0.20	−0.24	−0.28	−0.28	−0.10	0.03	0.03	−0.04	0.04
Spring	0.52	−0.71	−0.29	0.23	−0.08	−0.19	–	−0.28	−0.01	0.02	−0.08	−0.13	0.20	0.27	0.10	0.07	0.22
Growing season	0.27	−0.67	−0.52	−0.14	0.01	−0.33	–	−0.27	−0.17	−0.20	−0.29	−0.29	−0.18	0.03	0.02	−0.04	0.03
Summer	0.17	−0.67	−0.54	−0.47	−0.30	−0.51	–	−0.39	−0.44	−0.46	−0.31	−0.35	−0.29	−0.05	−0.03	−0.10	0.05

ε_{met} denotes the average deuterium fractionation by metabolic processes at glucose H[1] and H[2] ($\pm SE = 3.4$‰, $n \geq 3$). Data for the calculation of ε_{met} were acquired for tree-ring glucose of *Pinus nigra* laid down from 1983 to 1995 at a site in the Vienna Basin. Climate parameters: *VPD*, air vapour pressure deficit; *PRE*, precipitation; *PDSI*, the self-calibrating Palmer drought severity index (Wells *et al.*, 2004); *TMP*, air temperature; *SD*, sunshine duration; *RAD*, global radiation; C_a, atmospheric CO_2 concentrations; *SPEI*, the standardised precipitation–evapotranspiration index calculated for different timescales (1–48 months) (Vicente-Serrano *et al.*, 2010). Integration periods for the calculation of climate parameters: January to December, year; March to May, spring; March to November, growing season (Wieloch *et al.*, 2018); and June to July, summer. Significance levels: < 0.05, light blue; < 0.01, blue.

Table 3 Estimated coefficients of the ε_{met} change point model.

Coefficient	Estimate	SE*	Lower 95% CI	Upper 95% CI	P-value*
β_1	1801.97	479.02	863.10	2740.85	<0.001
β_2	−0.56599	0.17577	−0.91051	−0.22147	<0.01
β_3	−4.1851	1.4164	−6.9613	−1.4090	<0.01
β_4	−1722.11	479.90	−2662.71	−781.51	<0.001
β_5	0.58782	0.17749	0.23993	0.93571	<0.001
β_6	4.2138	1.4574	1.3573	7.0703	<0.01
e	−0.70310	0.05296	−0.80690	−0.59930	$<10^{-15}$

A change point model was fitted to measured ε_{met} data ($R^2 = 0.94$, $P < 10^{-15}$, $n = 31$, Eqn 7) (Fong et al., 2017). ε_{met} denotes the average deuterium fractionation by metabolic processes at glucose H^1 and H^2 ($\pm SE = 3.5‰$, $n \geq 3$). Data for the calculation of ε_{met} were acquired for tree-ring glucose of *Pinus nigra* laid down from 1961 to 1995 at a site in the Vienna Basin. β_1 to β_6, and e denote model coefficients (Eqn 7). SE and CI denote the standard error and confidence interval, respectively. Asterisks mark estimations, which assume that bootstrap sampling followed a normal distribution.

$$\varepsilon_{met} = \beta_1 + \beta_2 z_1 + \beta_3 z_2 + \beta_4 I(x > e) + \beta_5 z_1 I(x > e)$$
$$+ \beta_6 z_2 I(x > e) \qquad \text{Eqn 7}$$

where β_1 to β_6 are model coefficients, z_1 is March-to-June *PRE*, z_2 is annual C_a, x is the trend of the growing-season 48-month *SPEI* used as change point variable (Fig. 3a, dotted black line), and e is the change point value. If $x > e$, then $I(x > e)$ equals 1, else $I(x > e)$ equals 0. The fitted model explains 94% of the variability in ε_{met} and is highly significant ($P < 10^{-15}$, $n = 31$). All explanatory variables and the change point contribute significantly (Table 3). The estimated change point is at $-0.7 \pm 0.05SE$ corresponding to mild long-term drought ($P < 10^{-15}$, Table 3; Fig. 3a). The presence/absence and directionality of modelled ε_{met} relationships with precipitation and atmospheric CO_2 concentration agree with findings given above (Tables 1–3). In contrast to the model without response change point (Fig. 3b), the change point model captures the variability in the entire ε_{met} data set (Fig. 3c). Thus, this integrated change point model corroborates the following findings. First, ε_{met} exhibits a response change point. Below this change point, ε_{met} is largely constant with values of c. 96‰. Above the change point, ε_{met} variability is high. Second, change point crossing may require long-term drought beyond a critical level. Third, March-to-July precipitation and annual atmospheric CO_2 concentration may govern ε_{met} variability in short timescales when long-term drought is beyond the critical level. Note, all relationships indicated by modelling require experimental confirmation in controlled settings.

Variability in δD_g is predominantly controlled by fractionating metabolic processes

Metabolic fractionations in δD_1 and δD_2 have a strong weight on whole-molecule D variability, δD_g. Variance partitioning shows that δD_1 and δD_2 together account for 71% of the variance in δD_g (Fig. 2d). By contrast, δD_3 to δD_{6R} each accounts for 5.8% on average. Assuming the variability in δD_3 to δD_{6R} reflects the combined influence of nonmetabolic fractionation processes affecting all δD_i, such as leaf water D enrichment, metabolic fractionations in δD_1 and δD_2 together account for 59.4% of the variance in δD_g (71%−2 × 5.8%).

When years affected by metabolic fractionation are considered exclusively (green dots in Fig. 2c), metabolic fractionations in δD_1 and δD_2 together account for 74.2% of the variance in δD_g (Notes S5). After excluding the period affected by metabolic fractionation from the analysis (1983–1995), all δD_i exhibit similar degrees of variance and contribute similar to δD_g (Notes S6) consistent with expectations related to nonmetabolic fractionation processes. In conclusion, here, δD_g variability is predominantly controlled by fractionating metabolic processes unaccounted for in current models. Note, our estimations implicitly assume invariability of metabolic fractionations in δD_3 to δD_{6R}. This simplifies actual conditions and results in underestimation of the influence of metabolic fractionations on δD_g.

Altered metabolism is associated with below-average yet not exceptionally low growth

Metabolic changes as reflected by changes in metabolic fractionation may impact on growth. To test this, we investigated the relationship between ε_{met} and tree-ring width. We found that when the fractionating metabolic processes were upregulated, significantly more narrow tree rings were formed compared with those when they were downregulated (Fig. 3d, one-tailed t-test: green vs black circles, 0.75 vs 0.99 mm, $P < 0.05$, $n = 9$ and 22). Thus, altered metabolism is associated with below-average growth. However, equally narrow tree rings were formed in > 50% of the years in which the fractionating metabolic processes were downregulated (Fig. 3d; tree-ring widths < 0.99 mm, $n = 12$). Thus, upregulations of the fractionating metabolic processes are not associated with exceptional growth declines.

Discussion

ε_{met}: An isotope biomarker reports metabolic changes and drought

Here, we found highly variable metabolic fractionation signals at glucose H^1 and H^2 (Figs 1, 2). We approximated these signals by calculating ε_{met} (Eqn 5) and propose ε_{met} is a sensitive isotope

biomarker reflecting changes in plant metabolism. Furthermore, we found a change point in ε_{met} (Step 1; Fig. 3a–c) suggesting ε_{met} features a two-state property. This property promises unambiguous identification of alternate metabolic states: a stable state where the fractionating metabolic processes remain downregulated, and a state where these processes are upregulated (upon crossing a change point). By contrast, other biomarkers develop in a purely linear manner with indistinct transitions between states hindering attempts to ascertain plant functioning. While the mechanisms behind other biomarkers in plant archives often remain elusive, ε_{met} can be (1) linked to specific physiological processes and (2) incorporated into fractionation models (see later). Upon process elucidation, ε_{met} may help to find plants with the make-up to support crucial ecosystem services such as food and resource security.

As indicated by modelling, atmospheric CO_2 concentrations and drought exert control over ε_{met} in *Pinus nigra* studied here (Tables 1–3; Fig. 3a–c). Values of $\varepsilon_{met} > 105‰$ indicate long-term drought events affecting plant metabolism (Fig. 3a–c). Given careful sample selection (e.g. designed to avoid bias related to tree age), this may enable identification of historical occurrences. Fitting a model to ε_{met} values $> 105‰$ (Fig. 3b, $\varepsilon_{met} = 1802 - 0.566PRE - 4.185C_a$) may enable analyses of metabolic effects of short-term drought and C_a during long-term drought events (by interpretation of the respective model terms), and reconstructions of short-term drought events during long-term drought events (by solving for *PRE* with historical C_a data available).

Pinus nigra can access water from upper soil layers and from deep water sources (Stokes *et al.*, 2002; Peñuelas & Filella, 2003). Accordingly, at our study site, metabolic responses apparently require long-term drought (possibly involving groundwater depletion). In the absence of long-term drought, ε_{met} is blind to variability in short-term drought (possibly involving low soil moisture) and C_a (Fig. 3a–c). By contrast, species without groundwater access may provide this information. Lastly, ε_{met} may not always report drought, but it may always report source-limited growth conditions (cf. Wieloch *et al.*, 2022a).

The role of leaf intercellular CO_2 concentrations

As indicated by modelling, upregulations of the fractionating metabolic processes occur in response to drought, yet high atmospheric CO_2 concentrations exert counteracting effects (Tables 1–3; Fig. 3a–c). Isohydric plant species such as *Pinus nigra* respond to drought by closing their stomata (Sade *et al.*, 2012). This impedes CO_2 uptake and promotes low intercellular CO_2 concentrations, C_i. By contrast, increasing C_a promotes increasing C_i. Thus, upregulations of the fractionating metabolic processes may be mediated by low C_i. In principle, whole-molecule stable carbon isotope ratios of plant organic matter, $\delta^{13}C$, enable C_i estimations because ^{13}C fractionation during carbon uptake is related to C_i/C_a (Farquhar *et al.*, 1982; Evans *et al.*, 1986). However, in the samples studied here, processes that are independent of carbon uptake fractionation control $\delta^{13}C$ at three

out of six glucose carbon positions (Wieloch *et al.*, 2018, 2021b, 2022b). Therefore, we decided against using $\delta^{13}C$-derived C_i estimates to test this hypothesis.

Stable isotope methodology

Variability in δD_g is predominantly controlled by metabolic fractionation at glucose H^1 and H^2 (Fig. 2d). Since δD_g can be measured by high-throughput isotope ratio mass spectrometry, a technique accessible to numerous laboratories, we investigated possibilities to (1) detect δD_g data sets affected by metabolic fractionation; (2) separate δD_g data points affected by metabolic fractionation from other data points; and (3) retrieve information from δD_g about metabolic fractionation (Notes S7).

We found our δD_g data set holds clues to effects by metabolic fractionation at glucose H^1 and H^2 (Notes S7). Furthermore, the separation of δD_g data points affected by metabolic fractionation from other data points seems feasible yet not with high confidence. Discarding data sets/data points affected by metabolic fractionation at glucose H^1 and H^2 may improve δD_g analyses of nonmetabolic fractionation processes. However, analytical results will be impaired by other metabolic fractionations.

Modelling ε_{met}, we found both a response change point marking the onset of a period with conditions favourable for upregulation of metabolic fractionation processes and environmental dependences of upregulation (Table 3; Eqn 7; Fig. 3c). Applying this model to δD_g, we found the same change point, but the environmental dependences of upregulation were not sufficiently constrained for interpretation (Notes S7). Thus, by itself, δD_g analysis of glucose does not yield robust information about the environmental dependences of metabolic fractionation at H^1 and H^2. However, in combination with modelled or measured leaf water δD values, information on overall metabolic fractionation may be retrieved (cf. Cormier *et al.*, 2018). By contrast, resolving information about different metabolic fractionations requires the intramolecular approach.

Current δD_g models describe metabolic fractionations as being constant (Roden *et al.*, 2000). As shown here, this is inadequate for plants grown under dry conditions where metabolic fractionations can exert predominant control over δD_g variability (Fig. 2d). Thus, to model plant D abundance over the whole range of environmental conditions, metabolic fractionations need to be incorporated as variables, which requires detailed knowledge about underlying processes.

Metabolic fractionation processes known to affect tree-ring glucose H^1 and H^2 cannot explain our findings. Specifically, *Picea abies* reportedly exhibits similar heterotrophic hydrogen exchange rates at tree-ring glucose H^1 and H^2 (*c.* 42%) (Augusti *et al.*, 2006). Since *Pinus nigra* as a close relative can be expected to behave similarly, heterotrophic hydrogen exchange at these positions cannot cause pronounced deviations from slope = 1 as observed for the δD_1-δD_2 regression (Fig. 2c). Therefore, we will now derive experimentally testable theories on the metabolic origins of the fractionation signals reported here.
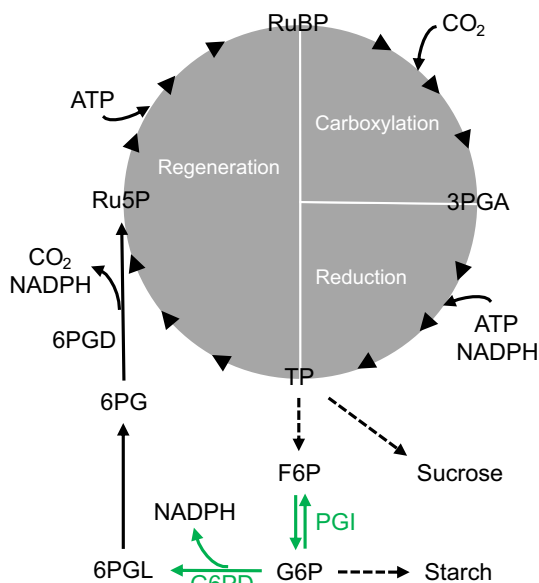
Fig. 4 Sucrose-to-starch carbon partitioning and anaplerotic carbon flux into the Calvin–Benson cycle. Green: enzyme reactions proposedly introducing D isotope signals at glucose H[1] and H[2]. G6PD has a kinetic isotope effect of $\alpha_D = k_H/k_D = 2.97$ (Hermes *et al.*, 1982), while PGI has a kinetic isotope effect of 2.22 in the F6P to G6P direction and an equilibrium isotope effect of 1.11 in G6P (Rose & O'Connell, 1961; Wieloch *et al.*, 2022a). Dashed arrows: intermediate reactions not shown. Enzymes: 6PGD, 6-phosphogluconate dehydrogenase; G6PD, glucose-6-phosphate dehydrogenase; and PGI, phosphoglucose isomerase. Metabolites: 3PGA, 3-phosphoglycerate; 6PG, 6-phosphogluconate; 6PGL, 6-phosphogluconolactone; ATP, adenosine triphosphate; F6P, fructose 6-phosphate; G6P, glucose 6-phosphate; NADPH, nicotinamide adenine dinucleotide phosphate; Ru5P, ribulose 5-phosphate; RuBP, ribulose 1,5-bisphosphate; and TP, triose phosphates (glyceraldehyde 3-phosphate, dihydroxyacetone phosphate).

Theory 1. Isotope fractionation related to sucrose-to-starch carbon partitioning

We found a highly variable metabolic fractionation signal at tree-ring glucose H[2] (ε_{met} at H[2]: SD *c.* ±79‰, range *c.* 260‰, $n = 31$), which occurs upon the crossing of a response change point (Fig. 3a–c). At the leaf level, tree-ring glucose has two precursors, starch and sucrose. Growing *Phaseolus vulgaris* and *Spinacia oleracea* under optimal conditions, Schleucher *et al.* (1999) reported D depletions at glucose H[2] of leaf starch relative to sucrose of 333‰ and 500‰, respectively. This difference may contribute to the signal at tree-ring glucose H[2] when the relative flux of assimilated carbon into starch and sucrose changes (Fig. 4). Sucrose-to-starch carbon partitioning ratios are controlled primarily by the rate of carbon assimilation (Sharkey *et al.*, 1985) and were shown to increase with decreasing assimilation rates (Sharkey *et al.*, 1985), decreasing C_i (Sharkey *et al.*, 1985), decreasing light (Sharkey *et al.*, 1985; Quick *et al.*, 1989) and increasing drought (Quick *et al.*, 1989, 1992; Vassey & Sharkey, 1989). Reported responses are functionally coherent and qualitatively consistent across all species studied. Furthermore, responses of sucrose-to-starch carbon partitioning to ecophysiological changes exhibit change points. For instance, in leaves of *Phaseolus*

vulgaris, the sucrose-to-starch carbon partitioning ratio was found to be largely constant at $C_i \geq 150$ ppm yet increases below this change point from *c.* 0.5 to *c.* 4 (Sharkey *et al.*, 1985). Thus, as C_i drops below the change point, the relative contribution of leaf sucrose to tree-ring glucose biosynthesis may increase, and tree-ring glucose H[2] may gradually approach the higher relative D abundance of leaf sucrose.

Theory 2. Isotope fractionation related to anaplerotic carbon flux into the Calvin–Benson cycle

Metabolic fractionation signals at tree-ring glucose H[1] and H[2] are closely related (Fig. 2a,c). We propose this is due to (1) isotope fractionation related to anaplerotic carbon flux into the Calvin–Benson cycle (CBC) affecting both positions; and (2) dependences of both anaplerotic carbon flux into the CBC and sucrose-to-starch carbon partitioning on the rate of carbon assimilation.

Sharkey & Weise (2016) proposed the CBC is anaplerotically refilled by injection of five-carbon sugar phosphates from the stromal pentose phosphate pathway with glucose 6-phosphate (G6P) as precursor (Fig. 4). Primary flux control is believed to be exerted at the level of stromal phosphoglucose isomerase (PGI), which catalyses interconversions between fructose 6-phosphate (F6P) and G6P. Under optimal growth conditions, the PGI reaction is strongly removed from equilibrium on the side of F6P resulting in low stromal G6P concentrations (Dietz, 1985; Gerhardt *et al.*, 1987; Kruckeberg *et al.*, 1989; Schleucher *et al.*, 1999). Proposedly, low G6P concentrations restrict the anaplerotic flux (Sharkey & Weise, 2016). However, as the PGI reaction shifts towards equilibrium and G6P synthesis, anaplerotic flux into the CBC is believed to increase (Sharkey & Weise, 2016). This involves stromal glucose-6-phosphate dehydrogenase (G6PD), the first enzyme of the pentose phosphate pathway. In the light, G6PD is downregulated via redox regulation by thioredoxin (Née *et al.*, 2009). However, downregulation can be allosterically reversed by increasing G6P concentrations (Cossar *et al.*, 1984; Preiser *et al.*, 2019).

Phaseolus vulgaris and *Spinacia oleracea* grown under optimal conditions exhibit pronounced D depletions at glucose H[2] of leaf starch relative to sucrose (as mentioned in the previous section) (Schleucher *et al.*, 1999). These depletions were attributed to the stromal PGI reaction being more strongly removed from equilibrium ([G6P]/[F6P] = 3.31) than the cytosolic PGI reaction (Dyson & Noltmann, 1968; Schleucher *et al.*, 1999). Thus, as the stromal PGI reaction shifts towards equilibrium, H[2] of stromal G6P and its derivatives including leaf starch and tree-ring glucose may become less D-depleted. Furthermore, G6PD catalyses the irreversible conversion of G6P to 6-phosphogluconolactone and was shown to have a strong D isotope effect *in vitro* ($\alpha = 2.97$) (Hermes *et al.*, 1982). Thus, upregulation of the anaplerotic flux may cause D enrichments at H[1] of stromal G6P and its derivatives.

As indicated by modelling, glucose H[1] and H[2] become D-enriched as drought increases and C_a decreases beyond a change point (Tables 1–3; Fig. 3a–c). Increasing drought and decreasing

C_a may cause decreasing C_i (as mentioned in a previous section), which may result in decreasing carbon assimilation. As carbon assimilation decreases below a change point, the stromal PGI reaction shifts towards equilibrium and G6P concentrations increase (Dietz, 1985). This may cause increasing G6PD activity and anaplerotic flux. Thus, expanding theory by Sharkey & Weise (2016), we propose anaplerotic flux into the CBC is upregulated in response to decreasing carbon assimilation, C_i and C_a, and increasing drought beyond a change point.

Analysis of intramolecular $^{13}C/^{12}C$ ratios of the samples studied here has already provided evidence consistent with anaplerotic flux into the CBC at high VPD (Wieloch *et al.*, 2018). These authors explained a strong common ^{13}C signal at tree-ring glucose C-1 and C-2 by anaplerotic flux changes. For shifts of the PGI reaction towards equilibrium, they predicted $^{13}C/^{12}C$ increases at C-1 and C-2 at a ratio of 2.25 and found a ratio of 2.74 (+1.35SE, −0.60SE) confirming their prediction. However, changes in sucrose-to-starch carbon partitioning would have the same effect. Furthermore, two recent studies report isotope and gas exchange evidence consistent with anaplerotic flux in *Helianthus annuus* at low C_i (Wieloch *et al.*, 2021a, 2022a). That said, other mechanisms than those discussed here may contribute to the signals at tree-ring glucose H^1 and H^2. This includes carbon flux into the oxidative branch of the cytosolic pentose phosphate pathway, shifts of the cytosolic PGI reaction and secondary isotope effects both in leaf and in tree-ring cells.

Metabolic fractionation signals at H^1 and H^2: a general phenomenon in C_3 plants?

Cormier *et al.* (2018) grew six phylogenetically diverse angiosperms under varying C_a. For leaf α-cellulose, these authors reported average whole-molecule ε_{met} increases of *c.* 20‰ in response to C_a decreases from 280 to 150 ppm, yet no significant change above 280 ppm. Hence, their observations are qualitatively in line with ours (Tables 1–3; Fig. 3a–c). However, our data show an average ε_{met} increase at tree-ring glucose H^1 and H^2 of up to 150‰ (Fig. 2b). Assuming *c.* 40% heterotrophic hydrogen exchanges as observed at these positions in *Picea abies* (Augusti *et al.*, 2006), we calculate an undiluted leaf-level increase of *c.* 250‰ (150‰/60 × 100), which corresponds to a whole-molecule increase of *c.* 70‰ (2 × 250‰/7). Thus, ε_{met} increases in the gymnosperm *Pinus nigra* are considerably larger than the *c.* 20‰ angiosperm average effect reported by Cormier *et al.* (2018). Additionally, whole-molecule data have a limited interpretability (cf. 'Introduction') and effects reported by Cormier *et al.* (2018) may be located at either of the seven H-C positions within α-cellulose glucose. Thus, it remains uncertain whether the fractionation signals reported here occur generally in C_3 plants.

Conclusion

Stable isotope analysis on plant archives such as tree rings may convey information (*inter alia*) about plant acclimation and adaptation (e.g. to CO_2 fertilisation), biosphere–atmosphere

CO_2 exchange and palaeoclimate trends. This long-term perspective is inaccessible to manipulation and monitoring experiments yet crucial for understanding plant and Earth system functioning. The better we understand plant isotope fractionation, the more information can be retrieved from archives (at higher quality). The present paper and recent studies on metabolic fractionation (Wieloch et al., 2018, 2021a,d,c; Ladd *et al.*, 2021) show there is much room for improvement. Thus, we recommend pushing the development of intramolecular isotope methodology.

Author contributions

TW and JS conceived the study. TW led the research. TW, MG, HS, JS and IE collected and prepared the samples and acquired data. TW and JY analysed the data. TW developed theories about the origin of reported isotope signals. TW wrote the paper with input from AA, HS, JS and JY.

ORCID

Angela Augusti https://orcid.org/0000-0002-9591-693X
Michael Grabner https://orcid.org/0000-0002-5220-721X
Jürgen Schleucher https://orcid.org/0000-0002-4815-3466
Henrik Serk https://orcid.org/0000-0003-4803-3664
Thomas Wieloch https://orcid.org/0000-0001-9162-2291
Jun Yu https://orcid.org/0000-0001-5673-620X

Data availability

The data that support the findings of this study are available from the corresponding author upon reasonable request.

References

Abtew W, Melesse AM. 2013. Chapter 5 – vapor pressure calculation methods. *Evaporation and evapotranspiration.* Dordrecht, the Netherlands: Springer, 53–62.

Augusti A, Betson TR, Schleucher J. 2006. Hydrogen exchange during cellulose synthesis distinguishes climatic and biochemical isotope fractionations in tree rings. *New Phytologist* **172**: 490–499.

Betson TR, Augusti A, Schleucher J. 2006. Quantification of deuterium isotopomers of tree-ring cellulose using Nuclear Magnetic Resonance. *Analytical Chemistry* **78**: 8406–8411.

Cernusak LA, Barbour MM, Arndt SK, Cheesman AW, English NB, Feild TS, Helliker BR, Holloway-Phillips MM, Holtum JAM, Kahmen A *et al.* 2016. Stable isotopes in leaf water of terrestrial plants. *Plant, Cell & Environment* 39: 1087–1102.

Chen Y, Helliker BR, Tang X, Li F, Zhou Y, Song X. 2020. Stem water cryogenic extraction biases estimation in deuterium isotope composition of plant source water. *Proceedings of the National Academy of Sciences, USA* 117: 33345–33350.

Cormier M-A, Werner RA, Sauer PE, Gröcke DR, Leuenberger MC, Wieloch T, Schleucher J, Kahmen A. 2018. ^{2}H-fractionations during the biosynthesis of carbohydrates and lipids imprint a metabolic signal on the δ^2H values of plant organic compounds. *New Phytologist* 218: 479–491.

Cossar JD, Rowell P, Stewart WDP. 1984. Thioredoxin as a modulator of glucose-6-phosphate dehydrogenase in a N_2-fixing cyanobacterium. *Microbiology* 130: 991–998.

Craig H, Gordon LI. 1965. Deuterium and oxygen 18 variations in the ocean and the marine atmosphere. In: Tongiorgi E, ed. *Stable isotopes in oceanographic studies and paleotemperatures*. Pisa, Italy: Consiglio nazionale delle ricerche, Laboratorio di geologia nucleare, 9–130.

Dietz K-J. 1985. A possible rate-limiting function of chloroplast hexosemonophosphate isomerase in starch synthesis of leaves. *Biochimica et Biophysica Acta* 839: 240–248.

Dyson JE, Noltmann EA. 1968. The effect of pH and temperature on the kinetic parameters of phosphoglucose isomerase. Participation of histidine and lysine in a proposed dual function mechanism. *Journal of Biological Chemistry* 243: 1401–1414.

Ehlers I, Augusti A, Betson TR, Nilsson MB, Marshall JD, Schleucher J. 2015. Detecting long-term metabolic shifts using isotopomers: CO_2-driven suppression of photorespiration in C_3 plants over the 20th century. *Proceedings of the National Academy of Sciences, USA* 112: 15585–15590.

Evans JR, Farquhar GD, Sharkey TD, Berry JA. 1986. Carbon isotope discrimination measured concurrently with gas exchange to investigate CO_2 diffusion in leaves of higher plants. *Australian Journal of Plant Physiology* 13: 281–292.

Farquhar GD, Cernusak LA, Barnes B. 2007. Heavy water fractionation during transpiration. *Plant Physiology* 143: 11–18.

Farquhar GD, O'Leary MH, Berry JA. 1982. On the relationship between carbon isotope discrimination and the intercellular carbon dioxide concentration in leaves. *Australian Journal of Plant Physiology* 9: 121–137.

Flanagan LB, Comstock JP, Ehleringer JR. 1991. Comparison of modeled and observed environmental influences on the stable oxygen and hydrogen isotope composition of leaf water in *Phaseolus vulgaris* L. *Plant Physiology* 96: 588–596.

Fong Y, Huang Y, Gilbert PB, Permar SR. 2017. chngpt: threshold regression model estimation and inference. *BMC Bioinformatics* 18: 454.

Frank DC, Poulter B, Saurer M, Esper J, Huntingford C, Helle G, Treydte K, Zimmermann NE, Schleser G h, Ahlström A *et al.* 2015. Water-use efficiency and transpiration across European forests during the Anthropocene. *Nature Climate Change* 5: 579–583.

Gerhardt R, Stitt M, Heldt HW. 1987. Subcellular metabolite levels in spinach leaves: regulation of sucrose synthesis during diurnal alterations in photosynthetic partitioning. *Plant Physiology* 83: 399–407.

Gray J, Song SJ. 1984. Climatic implications of the natural variations of D/H ratios in tree ring cellulose. *Earth and Planetary Science Letters* 70: 129–138.

Hermes JD, Roeske CA, O'Leary MH, Cleland WW. 1982. Use of multiple isotope effects to determine enzyme mechanisms and intrinsic isotope effects. Malic enzyme and glucose 6-phosphate dehydrogenase. *Biochemistry* 21: 5106–5114.

Kahmen A, Hoffmann B, Schefuß E, Arndt SK, Cernusak LA, West JB, Sachse D. 2013. Leaf water deuterium enrichment shapes leaf wax n-alkane δD values of angiosperm plants II: observational evidence and global implications. *Geochimica et Cosmochimica Acta* 111: 50–63.

Köhler IH, Macdonald AJ, Schnyder H. 2016. Last-century increases in intrinsic water-use efficiency of grassland communities have occurred over a wide range of vegetation composition, nutrient inputs, and soil pH. *Plant Physiology* 170: 881–890.

Kruckeberg AL, Neuhaus HE, Feil R, Gottlieb LD, Stitt M. 1989. Decreased-activity mutants of phosphoglucose isomerase in the cytosol and chloroplast of *Clarkia xantiana*. *Biochemical Journal* 261: 457–467.

Ladd SN, Nelson DB, Bamberger I, Daber LE, Kreuzwieser J, Kahmen A, Werner C. 2021. Metabolic exchange between pathways for isoprenoid synthesis and implications for biosynthetic hydrogen isotope fractionation. *New Phytologist* 231: 1708–1719.

Leal S, Eamus D, Grabner M, Wimmer R, Cherubini P. 2008. Tree rings of *Pinus nigra* from the Vienna basin region (Austria) show evidence of change in climatic sensitivity in the late 20th century. *Canadian Journal of Forest Research* 38: 744–759.

Loader NJ, Walsh RP, Robertson I, Bidin K, Ong RC, Reynolds G, McCarroll D, Gagen M, Young GH. 2011. Recent trends in the intrinsic water-use efficiency of ringless rainforest trees in Borneo. *Philosophical Transactions of the Royal Society of London* 366: 3330–3339.

Martin GJ, Zhang BL, Naulet N, Martin ML. 1986. Deuterium transfer in the bioconversion of glucose to ethanol studied by specific labeling at the natural abundance level. *Journal of the American Chemical Society* 108: 5116–5122.

McKee TB, Doesken NJ, Kleist J. 1993. The relationship of drought frequency and duration to time scales. In: *Proceedings of the 8th conference on applied climatology*. Anaheim, CA, USA: American Meteorological Society, 179–184.

Melander LCS, Saunders WH. 1980. *Reaction rates of isotopic molecules*. New York, NY, USA: John Wiley & Sons.

Née G, Zaffagnini M, Trost P, Issakidis-Bourguet E. 2009. Redox regulation of chloroplastic glucose-6-phosphate dehydrogenase: a new role for f-type thioredoxin. *FEBS Letters* 583: 2827–2832.

Peñuelas J, Canadell JG, Ogaya R. 2011. Increased water-use efficiency during the 20th century did not translate into enhanced tree growth. *Global Ecology and Biogeography* 20: 597–608.

Peñuelas J, Filella I. 2003. Deuterium labelling of roots provides evidence of deep water access and hydraulic lift by *Pinus nigra* in a Mediterranean forest of NE Spain. *Environmental and Experimental Botany* 49: 201–208.

Preiser AL, Fisher N, Banerjee A, Sharkey TD. 2019. Plastidic glucose-6-phosphate dehydrogenases are regulated to maintain activity in the light. *Biochemical Journal* 476: 1539–1551.

Quick P, Siegl G, Neuhaus E, Feil R, Stitt M. 1989. Short-term water stress leads to a stimulation of sucrose synthesis by activating sucrose-phosphate synthase. *Planta* 177: 535–546.

Quick WP, Chaves MM, Wendler R, David M, Rodrigues ML, Passaharinho JA, Pereira JS, Adcock MD, Leegood RC, Stitt M. 1992. The effect of water stress on photosynthetic carbon metabolism in four species grown under field conditions. *Plant, Cell & Environment* 15: 25–35.

Roden JS, Ehleringer JR. 1999a. Observations of hydrogen and oxygen isotopes in leaf water confirm the Craig-Gordon model under wide-ranging environmental conditions. *Plant Physiology* 120: 1165–1174.

Roden JS, Ehleringer JR. 1999b. Hydrogen and oxygen isotope ratios of tree-ring cellulose for riparian trees grown long-term under hydroponically controlled environments. *Oecologia* 121: 467–477.

Roden JS, Ehleringer JR. 2000. Hydrogen and oxygen isotope ratios of tree ring cellulose for field-grown riparian trees. *Oecologia* 123: 481–489.

Roden JS, Lin G, Ehleringer JR. 2000. A mechanistic model for interpretation of hydrogen and oxygen isotope ratios in tree-ring cellulose. *Geochimica et Cosmochimica Acta* 64: 21–35.

Rose IA, O'Connell EL. 1961. Intramolecular hydrogen transfer in the phosphoglucose isomerase reaction. *Journal of Biological Chemistry* 236: 3086–3092.

Ross GJ. 2015. Parametric and nonparametric sequential change detection in R: the CPM package. *Journal of Statistical Software* 66: 1–19.

Sade N, Gebremedhin A, Moshelion M. 2012. Risk-taking plants: anisohydric behavior as a stress-resistance trait. *Plant Signaling & Behavior* 7: 767–770.

Saurer M, Spahni R, Frank DC, Joos F, Leuenberger M, Loader NJ, McCarroll D, Gagen M, Poulter B, Siegwolf RTW *et al.* 2014. Spatial variability and temporal trends in water-use efficiency of European forests. *Global Change Biology* 20: 3700–3712.

Schleucher J. 1998. Intramolecular deuterium distributions and plant growth conditions. In: Griffiths H, ed. *Stable isotopes – integration of biological,*

ecological and geochemical processes. Oxford, UK: Bios Scientific Publishers, 63–73.

Schleucher J, Vanderveer P, Markley JL, Sharkey TD. 1999. Intramolecular deuterium distributions reveal disequilibrium of chloroplast phosphoglucose isomerase. *Plant, Cell & Environment* **22**: 525–533.

Schmidt HL, Robins RJ, Werner RA. 2015. Multi-factorial *in vivo* stable isotope fractionation: causes, correlations, consequences and applications. *Isotopes in Environmental and Health Studies* **51**: 155–199.

Schmidt H-L, Werner RA, Eisenreich W. 2003. Systematics of ^{2}H patterns in natural compounds and its importance for the elucidation of biosynthetic pathways. *Phytochemistry Reviews* **2**: 61–85.

Sharkey TD, Berry JA, Raschke K. 1985. Starch and sucrose synthesis in *Phaseolus vulgaris* as affected by light, CO_2, and abscisic acid. *Plant Physiology* **77**: 617–620.

Sharkey TD, Weise SE. 2016. The glucose 6-phosphate shunt around the Calvin-Benson cycle. *Journal of Experimental Botany* **67**: 4067–4077.

Speer JH. 2010. *Fundamentals of tree-ring research*. Tucson, AZ, USA: The University of Arizona Press.

Stokes A, Fourcaud T, Hruska J, Cermák J, Nadyezdhina N, Nadyezhdin V, Praus L. 2002. An evaluation of different methods to investigate root system architecture of urban trees *in situ*: I. ground-penetrating radar. *Journal of Arboriculture* **28**: 2–10.

Vassey TL, Sharkey TD. 1989. Mild water stress of *Phaseolus vulgaris* plants leads to reduced starch synthesis and extractable sucrose phosphate synthase activity. *Plant Physiology* **89**: 1066–1070.

Vicente-Serrano SM, Beguería S, López-Moreno JI. 2010. A multiscalar drought index sensitive to global warming: the standardized precipitation evapotranspiration index. *Journal of Climate* **23**: 1696–1718.

Waterhouse JS, Switsur VR, Barker AC, Carter AHC, Robertson I. 2002. Oxygen and hydrogen isotope ratios in tree rings: how well do models predict observed values? *Earth and Planetary Science Letters* **201**: 421–430.

Wells N, Goddard S, Hayes MJ. 2004. A self-calibrating Palmer drought severity index. *Journal of Climate* **17**: 2335–2351.

Wieloch T, Augusti A, Schleucher J. 2021a. Anaplerotic flux into the Calvin-Benson cycle. Integration in carbon and energy metabolism of *Helianthus annuus*. bioRxiv 2021.07.30.454461.

Wieloch T, Augusti A, Schleucher J. 2022a. Anaplerotic flux into the Calvin-Benson cycle. Hydrogen isotope evidence for *in vivo* occurrence in C$_3$ metabolism. *New Phytologist*. 10.1111/nph.17957.

Wieloch T, Ehlers I, Yu J, Frank D, Grabner M, Gessler A, Schleucher J. 2018. Intramolecular ^{13}C analysis of tree rings provides multiple plant ecophysiology signals covering decades. *Scientific Reports* **8**: 5048.

Wieloch T, Sharkey TD, Werner RA, Schleucher J. 2022b. Intramolecular carbon isotope signals reflect metabolite allocation in plants. *Journal of Experimental Botany*. 10.1093/jxb/erac028.

Wieloch T, Werner RA, Schleucher J. 2021b. Carbon flux around leaf-cytosolic glyceraldehyde-3-phosphate dehydrogenase introduces a ^{13}C signal in plant glucose. *Journal of Experimental Botany* **72**: 7136–7144.

Yakir D, DeNiro MJ. 1990. Oxygen and hydrogen isotope fractionation during cellulose metabolism in *Lemna gibba* L. *Plant Physiology* **93**: 325–332.

Supporting Information

Additional Supporting Information may be found online in the Supporting Information section at the end of the article.

Notes S1 Statistical analyses.

Notes S2 Grouping of annual δD_i patterns of tree-ring glucose by HCA.

Notes S3 Histograms of ε_{met}.

Notes S4 Bivariate relationships of ε_{met} with precipitation and atmospheric CO_2 concentration.

Notes S5 Contributions of δD_i to the variance in δD_g after excluding data not affected by the fractionating metabolic processes.

Notes S6 Contributions of δD_i to the variance in δD_g after excluding data affected by the fractionating metabolic processes.

Notes S7 Metabolic fractionation at the whole-molecule level.

Please note: Wiley-Blackwell are not responsible for the content or functionality of any Supporting Information supplied by the authors. Any queries (other than missing material) should be directed to the *New Phytologist* Central Office.